Multi-slope Path Loss and Position Estimation with Grid Search and Experimental Results

G. M. Bianco, R. Giuliano, F. Mazzenga, G. Marrocco

***Abstract*—A transmitting device can be localized based only on the received signal strength (RSS) measured by receivers. Typical RSS-based algorithms assume the a priori knowledge of the path loss (PL) the signal undergoes in the search area. Recently, algorithms removing this assumption have been introduced based on statistical and nonlinear methods to solve the optimization problem required to estimate the transmitter's position. However, such nonlinear methods could not converge to the optimal solution, especially in scenarios characterized by multi-slope or angular dependent PL. This paper considers an exhaustive search algorithm (ESA) for network localization based on the weighted least square (WLS) minimization. The algorithm's effectiveness is assessed by simulation and compared with the derived Cramér-Rao lower bound (CRLB). From experiments with very noisy measurements in indoor and outdoor, the localization error with 200 PL measurements employing the LoRa protocol is 5 m, whereas algorithms assuming a single slope incur errors between 12 m and 47 m.**

***Index Terms*—Angular dependent PL, multi-slope PL, network localization, path loss, RSS localization.**

I. Introduction

In the last years, wireless networks became pervasive, ranging from wireless local area networks to wireless sensor networks and cellular networks. The localization of a radio frequency signal source (hereafter called *target*) in an area covered by a radio network is a crucial issue widely studied. Proposed strategies to localize the target are based on different techniques: angle-of-arrival (AoA, also known as direction-of-arrival, DoA), time-of-arrival (ToA), time-difference-of-arrival (TDoA) and received signal strength (RSS) [1]. Combined methods have been proposed, too, as DoA-RSS [2] and DoA-ToA [3] hybrid algorithms. Since AoA, ToA, and TDoA-based techniques require costly antenna arrays and synchronization, RSS-based methods are considered low requirements candidates for localization [4]. This paper focuses on range-based position estimation exploiting the RSS [5]. The effectiveness of these algorithms has been extensively analyzed and corroborated by theoretical and experimental results in many papers, e.g. [6], [7].

To assess the unknown position of one transmitter through RSS, it is required to have a network wherein the locations of some receivers, usually indicated as *anchor points*, are known. In the latest dense and ultra-dense 5G networks [8], the number of anchor points can increase significantly, as the number of available RSS measurements. Thanks to the higher number of anchor points, new RSS-based localization services can be created, especially to enable indoor navigation, which could greatly help visually impaired people [9]. In general, anchor points can move [10] to collect more RSS measurements. RSS-based localization systems have a large number of applications. For example, RSS-based localization techniques can be applied in ad-hoc networks to vehicle localization [11] or for surveillance purposes [12]. In the latter case, it is necessary to correctly detect the presence of the target while avoiding false alarms [13]–[15], and non-cooperative localization is required when the transmitting power is unknown [16].

This paper discusses an algorithm that can solve the RSS-based localization problems based on weighted least square (WLS) minimization. One application of the considered estimation technique has been presented in [17] using weighted data in a simple scenario with single-slope path loss (PL) propagation models obtained from experimental measurement campaigns. However, the localization algorithm has not been analyzed in terms of computational complexity, accuracy, run time, nor it has been tested experimentally. Most important, this is the first work studying the RSS-based localization with multi-slope [18]–[21] and/or angular dependent [22], [23] PL models. Single-slope PL models are not accurate in these complicated propagation environments resulting in higher localization errors [19], [24]. We assess the algorithm's performances through simulation, and we compare them with the derived Cramér-Rao lower bound (CRLB).

The paper is organized as follows. In section II, we review the works akin to this one, and we highlight the novelty introduced by the technique presented in this paper. In sec. III, we detail the considered PL model and

Giulio Maria Bianco and Gaetano Marrocco are with the Pervasive Electromagnetics Lab, University of Rome Tor Vergata, Rome, Italy. Email: *giulio.maria.bianco@uniroma2.it* (contact author)

Romeo Giuliano is with the Department of Engineering Science, Guglielmo Marconi University, Rome, Italy.

Franco Mazzenga is with the Department of Enterprise Engineering "Mario Lucertini", University of Rome Tor Vergata, Rome, Italy.

This paper has supplementary downloadable material available at https://ieee-dataport.org, provided by the authors. This material includes the log of the PL measurements collected by each anchor and a file explaining how to use them. The dataset is 84 kB in size, is composed of text files solely, and is available at http://dx.doi.org/10.21227/agyw-ws11

This is a pre-print of a paper accepted for publication on *IEEE Transactions on Signal and Information Processing over Networks* in 2021. Changes were made to this version by the publisher prior to publication. The final version of record is available at http://dx.doi.org/10.1109/TSIPN.2021.3106693

TABLE I
RSS-UDPG localization algorithms most similar to the one described in this paper and respective validation areas.

Algorithm	**Exhaustive search**	**PL(d_0) estimation**	**Multi-slope PL**	**Simulated validation (largest area considered; normalized by d_0)**	**Experimental validation (largest test area)**
This work	Yes	Yes	Yes	Yes (200 × 200)	Yes (62 m × 58 m)
[25]	Yes	Yes	No	Yes (1000 × 2000)	No
[26]	Yes	No	No	Yes (3 × 3)	No
[27]	Yes	No	No	Yes (10 × 10)	No
[28]	Yes	No	No	No	Yes (15 m × 15 m)
[29]	No	Yes	No	Yes (20 × 20)	No
[30]	No	Yes	No	Yes (40 × 40)	No
[31]	No	Yes	No	No	Yes (Not reported)
[32]	No	No	No	Yes (50 × 50)	Yes (8 m × 12 m)
[33]	No	No	No	Yes (20 × 20)	No
[34]	No	No	No	Yes (circle of radius 20)	No
[35]	No	No	No	Yes (circle of radius 50)	No
[24]	No	No	No	Yes (50 × 50)	No
[36]	No	No	No	Yes (20 × 20)	No
[37]	No	No	No	Yes (15 × 10)	No

the method commonly used to measure PL. The algorithm and its computational complexity are discussed in sec. IV. In sec. V, two variations of the considered algorithm are introduced concerning the hierarchical search and the inclusion of PL angular dependence. In sec. VI, performances indexes are evaluated by simulations in different conditions and compared with the CRLB. Finally, the algorithm and classical methods assuming a single slope are experimentally tested in a setting wherein a dual-slope PL is expected (sec. VII). Conclusions and possible future directions are finally drawn in sec. VIII.

II. Related Works

Several RSS-based localization algorithms, such as [38] and [39], either require excellent knowledge of the radio propagation PL model for the considered area or are based on the adoption of the models in [40]. The assumption of accurate knowledge of the PL specific for the site is an oversimplification in many cases, leading to erroneous position estimates, mainly when the area's radio map is not updated to account for changes in the topology. Recently presented RSS-based localization methods jointly estimate both the transmitter's position and the PL model parameters to provide more accurate results. The algorithm discussed in this paper can be categorized in this second type of localization, which is usually indicated as "RSS-based with an unknown distance-power gradient (RSS-UDPG)" [34].

In [34], the RSS-UDPG problem is formulated and analyzed, assuming the propagation follows an unknown lognormal PL. A nonlinear optimization problem with three unknowns (i.e., the 2D coordinates of the target and the path loss exponent, PLE) is proposed. The corresponding nonlinear least square problem is solved using the Gauss-Newton (GN) algorithm and applying the Levenberg-Marquardt method.

In [31], a statistical approach is investigated for indoor RSS-UDPG navigation. The performances of the Metropolis-Hastings (MH) sampler and the Bayesian GN are compared with those of two classic methods, the statistical coverage areas (CA) and the weighted k-nearest neighbour (WKNN) algorithm. Both the MH and the Bayesian GN performed better than the CA but worse than the WKNN.

Reference [27] describes a grid-based RSS centralized localization. It considers that the PLE of each link is unknown and ranging between a minimum and a maximum value. A spatial grid is superimposed over the search area for the position of the unknown transmitter. Considering the RSS measurements received by a single anchor point, two distance values are evaluated using the minimum and the maximum PLE values. Every grid point whose distance from the anchor point is comprised between the two values is voted once. The voting procedure is repeated for each anchor point. Finally, the point of the grid having the most votes is the estimated position of the transmitter. This approach achieves a rough estimate of the PLE. Another grid-based process in [28] consists of varying the PLE tentatively so that the algorithm selects the pair (transmitter position, PLE), minimizing the least-squares difference with the data. It is assumed that $PL(d_0)$ (the PL at a reference distance d_0) is known and given as input in both cases.

Other techniques of addressing the RSS-UDPG localization are more different from the one proposed in this paper. In [35], a joint estimator of position and PL parameters based on the GN algorithm is studied, whereas a single cost function is minimized to perform the joint estimation in [24]. A maximum likelihood estimator on the transmitter position is employed with an exhaustive search algorithm (ESA) on the PLE in [26]. In [30], unscented transformation is applied. In [29], [32], [37], [41], two-step searches divide the PL estimation and localization problems. In [25], [36], the algorithms are based on RSS ratios, and ref. [25] performs an exhaustive search on the PLE value to estimate the location and the $PL(d_0)$. A convex relaxation algorithm is considered in [33], whereas several methods to estimate the PL without

relying on distance measurements are proposed in [42] to complete the classic RSS-based localization subsequently. Since for a fixed position of the transmitter the PL intercept and the PLE can be calculated analytically in closed-form [43], we restrict the exhaustive search to the transmitter's position. We show that the WLS RSS-based localization can be significantly extended to account for complex propagation scenarios, including multi-slope PL models and the eventual PL angular dependence, not addressed in the previous works. In particular, the WLS-RSS localization was usually considered a nonlinear optimization problem to solve through algorithms such as GN. These solving techniques can be hardly applied to complex PL scenarios, and their instability can cause them to fail.

The RSS-based localization techniques using WLS minimization are a well-studied topic. After an extensive review of the available literature, in Table I we indicate the works providing contributions that could be considered similar to those presented in this paper. In the same table, we also indicate the extensions of their validation areas.

III. Path Loss Models and Measurements

The classic narrowband radio propagation PL model for a receiver at a distance d from the transmitter (in dB) is

$$PL(d) = PL_m(d) + n_S, \tag{1}$$

where PL_m is the mean PL and n_S accounts for randomly variable shadowing, usually modeled as lognormal, with zero mean and standard deviation σ_S (in dB). The mean log-distance PL model $PL_m(d)$ can be generalized to a multi-slope model including multiple distance-power gradients [40], namely

$$PL_m(d) = \left\{ L_k + 10\gamma_k \cdot \log_{10}\left(\frac{d}{d_0}\right),\ d_k^{(c)} \le d < d_{k+1}^{(c)} \right\} \tag{2}$$

and $k = 1, 2, \ldots, K$, where γ_k is the k-th PLE, $d_{K+1}^{(c)} = \infty$, $d_1^{(c)} \ge d_0$, and $\{d_k^{(c)}\}$ are named *critical distances* [20], [21]. The d_0 is a reference distance, and the $\{L_k\}$ are the $PL_m(d_0)$ values. In the following, $d_1^{(c)} = d_0$ and $d_0 = 1$ m are assumed to simplify the notation.

The different PLEs γ_k, $k = 1, 2, \ldots, K$ in (2) account for the propagation in various mediums and different configurations of obstacles around the receiver, causing distinct multipath effects. From (2), the mean of the PL is expected to follow a piecewise-linear function [44], and the PL slope changes at distances $d_k^{(c)}$, $k = 1, 2, \ldots, K$. With the considered formulation, discontinuous behavior of the mean PL at the critical distances $d_k^{(c)}$ is allowed (Fig. 1). The model can be further generalized to include the eventual PL's angular dependence by introducing *critical angles* $\delta_k^{(c)}$ similar to the critical distances. In Table II, we report some references to other works considering empirical PL models, including multi-slope and/or angular dependence. All of these models can be re-formulated as in (2). From a thorough search of the relevant literature, we found $K \le 4$, albeit $K > 4$ is theoretically possible.

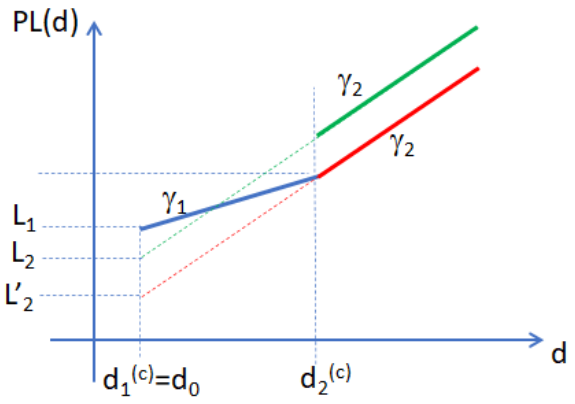

Fig. 1. A pictorial example of dual-slope PL models according to (2).

TABLE II
Selected empirical multi-slope path loss models.

Model	Environment (frequency)	K	Continuous model	Angular dependence
[45]	Indoor (900 MHz)	4	Yes	No
[46]	Urban (900 MHz)	4	No	Yes
[47]	Railway (28 GHz)	3	Yes	No
[48]	Indoor (27.5 GHz)	2	No	No
[49]	Orchad (5.8 GHz)	2	No	No
[50]	Tunnel (900 MHz)	2	No	No

In the current practice, the $PL(d)$ from a transmitter to a receiver at a distance d can be estimated from the RSSI (RSS indicator), and the signal-to-noise ratio (SNR) returned by the chip [17]

$$PL = P_T + G_T + G_R + 10 \cdot \log_{10}\left(1 + \frac{1}{SNR}\right) - RSSI, \tag{3}$$

where P_T is the transmission power, whereas G_T and G_R are the gains of the transmitting and receiving antennas, respectively. The variables in (3) are in the dB scale except for the SNR, which is in the linear scale. Measurements obtained from (3) can be used to estimate the mean PL model parameters, i.e. γ_k, L_k and the critical distances $\{d_k^{(c)}\}$ in (2) if the distance between the transmitter and receiver is known.

It is worth noticing that assuming P_T, G_T, and G_R are unknown but do not vary (for instance, omnidirectional transmitting and receiving antennas), the estimated PL in (2) would differ from the actual value by a constant, which can be accounted for in L_k. If these parameters are allowed to vary around their effective values randomly (e.g. multiple receivers with different characteristics in terms of antenna gain and losses), the fluctuations would introduce an additional noise in the PL measurements, which can be added to the shadowing fluctuations. This noise would

alter the evaluated L_k, whereas the algorithm can smooth the fluctuations.

IV. Localization Algorithm

In this section, the ESA is described, and its computational complexity is evaluated.

A. Exhaustive Search

Indicating with (x_T, y_T)[1] the unknown position of the transmitter, we assume M PL measurements are taken over the entire area and that for each PL measurement, the position of the receiver $P_R = \{(x_m, y_m)\}$, $m = 1, \ldots, M$, is known. The M PL measurements can be used to estimate the parameters of the mean PL model in (2) and the transmitter's position by minimizing the following WLS function

$$\varepsilon\left(\{L_k\}_{k=1}^K, \{\gamma_k\}_{k=1}^K, \{d_k^{(c)}\}_{k=1}^K, x_T, y_T\right) = \sum_{k=1}^{K}\sum_{n=1}^{N_k} w_{kn}\left|\overline{PL}_{kn} - L_k - 10\gamma_k \log_{10}\left(d_{kn}\right)\right|^2, \quad (4)$$

where w_{kn} is the weight of the $\overline{PL}_{kn}$ measure, N_k is the cardinality of the k-th subset, $k = 1, \ldots, K$ of PL measurements in P_R, including the PL values $\overline{PL}_{kn} \in P_R$ such that the distance d_{kn} between the receiver and the transmitter is $d_k^{(c)} \leq d_{kn} < d_{k+1}^{(c)}$ for $n = 1, 2, \ldots, N_k$. We have $M = N_1 + N_2 + \ldots + N_K$, and the partitioning of the M PL measurements into the K subsets to be used in (4) varies each time with the assumed transmitter's position. Hereafter, $w_{kn} = w = 1$ is implied for the sake of conciseness without any loss of generality.

The cost function (4) is non-convex and has multiple local minima [34]. However, it can become convex with respect to γ_k and L_k, $k = 1, \ldots, K$, when fixing the (x_T, y_T) pair. To minimize (4) for fixed K and assigned critical distances $d_k^{(c)}$, we first need to partition the available set of M measurements into the K subsets $\{\overline{PL}_{kn}\}$, $n = 1, \ldots, N_k$, $k = 1, \ldots, K$. For this purpose, we start by fixing the position (x_T, y_T) of the transmitter and then evaluate the set of distances $\{d_{mT}\}$, $m = 1, \ldots, M$ between the M measurements points and the transmitter. The m-th PL measurement is assigned to the k-th subset if $d_k^{(c)} \leq d_{mT} < d_{k+1}^{(c)}$. At the end of the partitioning process, we reindex with d_{kn} the N_k receivers' distances whose PL measurements have been included in the k-th subset following the previous criterion.

For the given (x_T, y_T) and the corresponding partition of the PL measurements, from (4), it can be observed that the optimal values of $\{L_k\}_{k=1}^K$ and the PLEs $\{\gamma_k\}_{k=1}^K$ can be determined in closed-form by solving the following K separated linear systems with two equations

$$\begin{cases} L_k N_k + 10\gamma_k \sum_{n=1}^{N_k} \log_{10}(d_{kn}) = \sum_{n=1}^{N_k} \overline{PL}_{kn} \\ L_k \sum_{n=1}^{N_k} \log_{10}(d_{kn}) + 10\gamma_k \sum_{n=1}^{N_k} \left(\log_{10}\left(d_{kn}\right)\right)^2 = \\ \qquad \sum_{n=1}^{N_k} \overline{PL}_{kn} \log_{10}(d_{kn}), \quad k = 1, \ldots, K \end{cases} \quad (5)$$

where $d_{kn} = \sqrt{(x_{kn} - x_T)^2 + (y_{kn} - y_T)^2}$, $n = 1, \ldots, N_k$. Solving (5) we obtain that for each k, $k = 1, \ldots, K$, the corresponding L_k and γ_k are

$$L_k = \frac{\sum_{n=1}^{N_k} \overline{PL}_{kn} - 10\gamma_k \sum_{n=1}^{N_k} \log_{10}(d_{kn})}{N_k} \quad (6)$$

and

$$\gamma_k = \frac{N_k \sum_{n=1}^{N_k} \overline{PL}_{kn} \log_{10}(d_{kn}) - \sum_{l=1}^{N_k} \overline{PL}_{kl} \sum_{n=1}^{N_k} \log_{10}(d_{kn})}{10 N_k \sum_{n=1}^{N_k} \left(\log_{10}(d_{kn})\right)^2 - 10\left(\sum_{n=1}^{N_k} \log_{10}(d_{kn})\right)^2}. \quad (7)$$

The K systems (5) should not be under-determined, and, in general, the number of available measurements for each one of the K systems needs to be higher than the number of the corresponding PL parameters to evaluate (6) and (7). In the presence of shadowing, the number of measurements $M \gg 2K + 1$ is required to achieve an accurate estimate of the position.

The previous procedure is based on the implicit knowledge of the transmitter position (x_T, y_T), which is unknown and must be determined to minimize (4). Therefore, we assume that (x_T, y_T) can vary over a spatial grid of candidate points, superimposed on the considered area by excluding the eventual positions where the transmitter cannot be. The overall minimization procedure can now be stated as follows, w.r.t. Fig. 2:

1) start from M PL measurements taken at known points (x_m, y_m), $m = 1, \ldots, M$ in the area;
2) assign the $K-1$ critical distances, $d_k^{(c)}$, $k = 2, \ldots, K$;
3) select the candidate point (x_T, y_T) in the grid and evaluate the distances of receivers d_{mT}, $m = 1, 2, \ldots, M$ from the selected transmitter point in the grid;
4) partition the set of the M PL measurements into the K subsets $\{\overline{PL}_{kn}\}$, $n = 1, \ldots, N_k$ assigning the measure $\overline{PL}_m$ to the k-th subset if the corresponding receiver distance d_{mT} is such that $d_k^{(c)} \leq d_{mT} < d_{k+1}^{(c)}$;
5) for each k, $k = 1, 2, \ldots, K$, calculate L_k and γ_k using (6) and (7), respectively;
6) evaluate the minimum least square error in (4) obtained with the selected (x_T, y_T) and the corresponding L_k and γ_k in (6) and (7) for $k = 1, \ldots, K$ obtained in the previous step, and store them;

[1]For simplicity, in the following, we consider the bidimensional case. Nevertheless, the procedure can be easily extended to the tridimensional case.

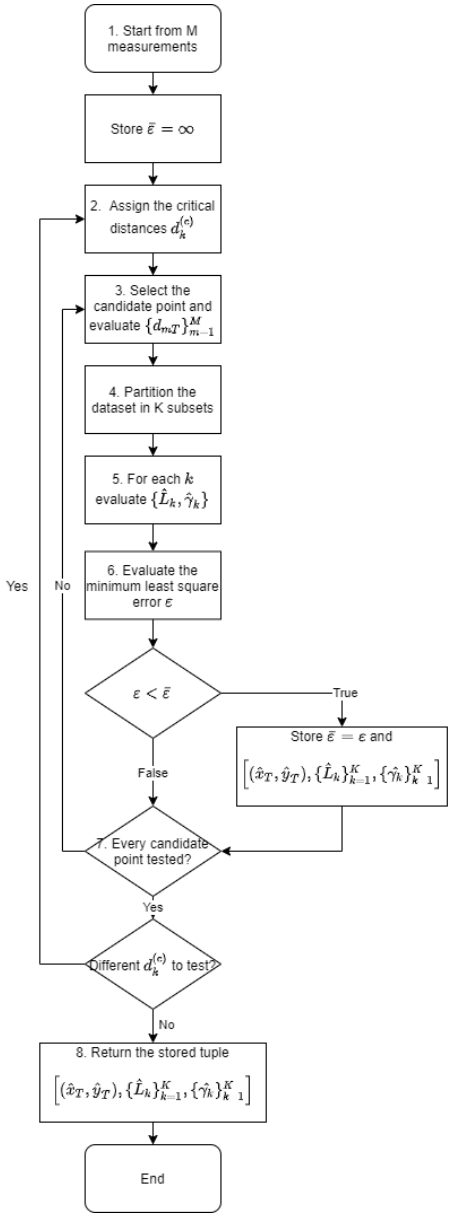

Fig. 2. Flow chart describing the proposed UDPG-RSS-based localization ESA.

7) repeat the calculation procedure from point 3) by selecting the next candidate transmitter point on the grid until all the points in the grid have been considered;
8) after the examination of all the candidate points, the tuple $\left[(\hat{x}_T, \hat{y}_T), \{\hat{L}_k\}_{k=1}^{K}, \{\hat{\gamma}_k\}_{k=1}^{K}\right]$ achieving the minimum least square error in (4) provides the best solution for minimizing (4).

We implicitly assumed the $K-1$ critical distances $d_k^{(c)}$ had been set. If $d_k^{(c)}$ are not available, it is possible to repeat the procedure by varying $d_k^{(c)}$ over a set of values taking into account that $d_0 = d_1^{(c)} < d_2^{(c)} < \ldots < d_K^{(c)}$. In the more common case when $K = 2$, we have one critical distance to set at every iteration of the optimization algorithm. Finally, we select the tuple $[\{\hat{d}_k^{(c)}\}_{k=1}^{K}, (\hat{x}_T, \hat{y}_T), \{\hat{L}_k\}_{k=1}^{K}, \{\hat{\gamma}_k\}_{k=1}^{K}]$ providing the absolute minimum of (4) concerning the configurations of critical distances $d_k^{(c)}$.

TABLE III
Terms contributing to the computational complexity.

Operation	Number of Multiplications
$\{\gamma_1, ..., \gamma_K\}$ evaluation	$2M + 7K$
$\{L_1, ..., L_K\}$ evaluation	$3K$
ε evaluation	$4M$
Overall complexity	$\mathcal{O}(Q \cdot n_P \cdot K \cdot M)$

B. Computational Complexity of the Algorithm

Let Q be the number of sets of $K-1$ elements, each containing the values of the critical distances $\{d_k^{(c)}\}_{k=1}^{K}$ to be considered in the position estimation. Let n_P be the number of candidate points on the grid to be analyzed in each algorithm iteration for a given set of critical distances. Calculations from point 3) in Fig. 2 are then repeated $Q \times n_P$ times. Accordingly, the evaluation of (6), (7) and of the corresponding values of the WLS error in (4) are carried out $Q \times n_P \times K$ times. In the case of a regular grid of candidate points uniformly spaced by Δ along the x and y axes, the number of grid points can be approximated as $n_P = \lceil A/\Delta^2 \rceil$ where A is the extension of the considered area and $\lceil \cdot \rceil$ is the lowest integer higher than the argument. Thus, in general, the computational complexity of the considered algorithm is polynomial with the number n_P of candidate points for fixed Q and K. The terms contributing to the computational complexity[2] are resumed in Table III.

V. Variations of the Algorithm

In this section, the reduction of the ESA computational complexity through hierarchical search and the partitioning accounting for the PL angular dependence are discussed.

A. Hierarchical Search

The basic algorithm detailed in the previous section assumes that the search of the transmitter position (x_T, y_T) is carried out over a grid of points. Considering a regularly spaced grid with points uniformly spaced along the x and y axes by Δ, for a given area A, the total number of points to be tested is

$$n_P = \left\lceil \frac{A}{\Delta^2} \right\rceil . \tag{8}$$

To reduce the number of candidate points n_P, the following hierarchical procedure can be adopted, exploiting the mostly monotonic behavior of (4) [Fig. 3(a)]. Accordingly, the search for the best candidate point is carried out in two steps. The procedure starts with a search over a coarse grid with points uniformly spaced

[2]We assumed logarithms are tabulated.

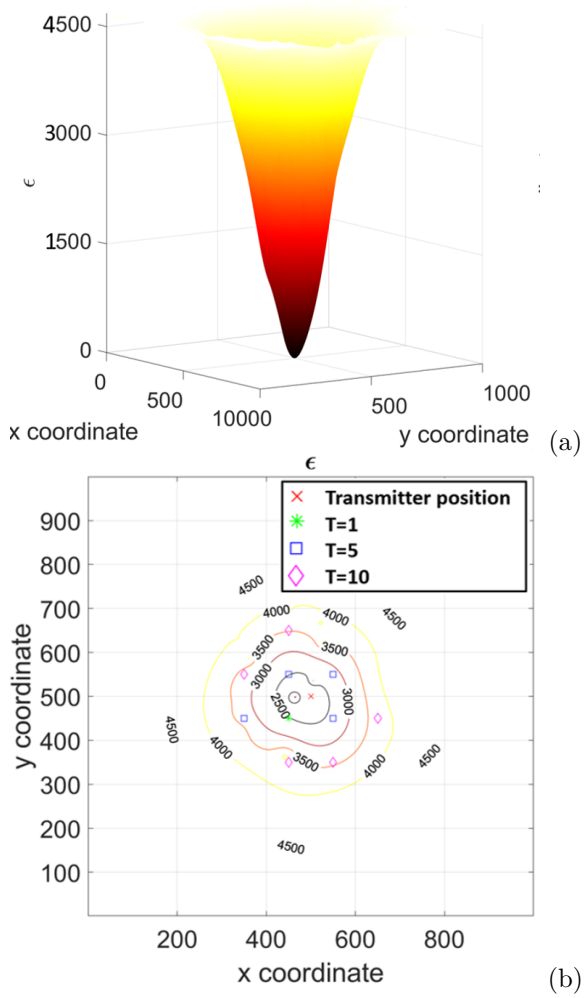

Fig. 3. (a) Error function ϵ evaluated from (4) when $M = 100$, $\sigma_S^2 = 12$ dB over a 1000 m $\times$ 1000 m search area (single-slope PL), and (b) corresponding contour plot and candidate points when varying T.

with a relatively large step $q\Delta$, where $q > 1$ is an integer. For the same area A, the number of candidate points is now proportional to $A/(q\Delta)^2 < n_P$. After the first search step, we order the WLS errors in (4) corresponding to the considered candidate points in ascending order. To start the second search stage, we select the T candidate points achieving the first T ordered WLS error values. Then, the search for the best transmitter position proceeds over T smaller grids, each centred around one of the selected T target points [Fig. 3(b)]. The spacing of points in these grids is reduced to Δ. For simplicity, considering square grids, we assume each one extends from $-m\Delta/2$ to $(m-1)\Delta/2$ along the x and y axes, and m is an integer. As an example, let us impose $m = 2q$. Therefore, the second search is carried out over (m^2-1) candidate points for each grid. In the considered two-step hierarchical search, the total number of candidate points can be approximated as

$$\alpha n_P \cong \frac{n_P}{q^2} + (m^2 - 1) \cdot T, \tag{9}$$

where $0 < \alpha < 1$.

Even in this simple case, the optimal set of parameters (q, m, T) depends on the specific search strategy, on the network topology, on how the grid is superimposed over the search area and on the characteristics of the radio propagation environment. Generally, the lower the α, the higher can be errors caused by the coarse grid step and the possibility of falling in one local minimum.

B. PL Angular Dependence

As shown in sec. IV, the considered algorithm introduces the partitioning of M available PL measurements. The partition depends on the critical distances and the position of the selected candidate point. Partitioning can be based on the critical angles, too, considering the PL measurements' angular dependence for each candidate point and the critical distances. For each candidate point, the subsets of PL measurements falling into one sector are now used to run the WLS minimization (Fig. 4). Even in this case, the minimization of the WLS can be run for each angular sector independently of the other sectors, and equations (6) and (7) are still valid provided the K subsets of PL measurements are properly redefined for each candidate point. Naturally, K accounts now also for the number of sectors considered in the minimization, and the algorithm can run multiple times by varying the critical angles if needed.

VI. Performance Analysis

In this section, the performance of the considered RSS-based position estimation algorithm is evaluated by simulations in terms of achievable accuracy. The numerical results are compared with the derived CRLB.

We impose $\Delta = 1$ m, and the transmitter's position randomly varies around $\pm\Delta/2$ in the horizontal and vertical directions near the search area's centre in each trial. M anchor points are then randomly positioned in the area. The corresponding PLs are generated by (1) and

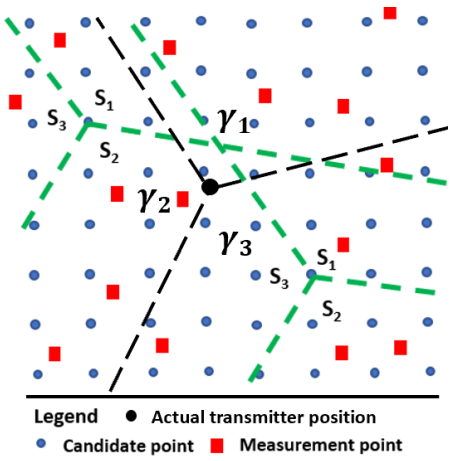

Fig. 4. A simple scheme of the angular partition of PL measurements with respect to each candidate point: a case of three sectors S_1, S_2, S_3.

TABLE IV
SIMULATION PARAMETERS USED TO GENERATE THE PL DATA FOR THE PERFORMANCE ANALYSIS. A SQUARE SEARCH AREA HAVING 200 m SIDE AND $L_k = L = 30$ dB ARE CONSIDERED.

PL model	PL Exponents	σ_S^2[dB]
Single-slope	$\gamma = 2$	$\{3, 12\}$
Dual-slope	$\gamma_1 = 2$,$\gamma_2 = 4$	3
Two angular sectors	$\gamma_1 = 2$,$\gamma_2 = 4$	3

(2), including shadowing, which is modeled as a zero-mean normal random variable with standard deviation σ_S as in (1). The following simulations are performed according to Table IV, and the results are averaged on 1000 trials. We consider the case $K = 2$ and generate half of the PL data per slope for simplicity. Moreover, we omit the standard deviations (STDs) corresponding to the average errors since, from our simulations, the STDs are primarily due to the shadow fading, and their values are slightly lower than the average errors themselves. Lastly, to evaluate the CRLB, we avoid anchor points' distributions resulting in badly conditioned or singular Fisher information matrixes (for example, anchor points along a line or placed on a circle around the target).

The analyses are repeated using single-step and hierarchical search. We select $q = m = 10$ and $T = 5$ as hierarchical search parameters, leading to $\alpha \cong 0.02$ from (9). The difference in the position estimate with and without hierarchical search is negligible.

A. Cramér-Rao Lower Bound

The CRLB expresses the minimum variance of unbiased estimators of deterministic parameters. From (2), the estimator $g_{kn}(\theta)$ can be expressed as

$$g_{kn}(x_n, y_n, \gamma_k, L_k) = L_k + 10\gamma_k \cdot \log_{10}\left(\frac{d_{kn}}{d_0}\right), \quad (10)$$

and $\theta = [x, y, \gamma_1, ..., \gamma_K, L_1, ..., L_K]^T$ is the unknown parameters vector. From [34], the PL observations $\overline{PL}_{kn}$ have a probability density function

$$f\left(\overline{PL}_{kn}; \theta\right) = \frac{1}{\sqrt{2\pi}\sigma_S} \exp\left\{-\frac{\left(\overline{PL}_{kn} - g_{kn}(\theta)\right)^2}{2\sigma_S^2}\right\}. \quad (11)$$

By assuming that the observations are statistically independent, the joint distribution of the observation matrix[3] $\overline{\mathbf{PL}}$ is

$$f\left(\overline{\mathbf{PL}}; \theta\right) = \prod_{k=1}^{K}\prod_{n=1}^{N_k} f\left(\overline{PL}_{kn}; \theta\right). \quad (12)$$

The CRLB is evaluated from the inverse of the Fisher information matrix

$$\mathbf{F} = -E\left[\nabla_\theta \left(\nabla_\theta \ln f(\overline{\mathbf{PL}}; \theta)\right)^T\right]. \quad (13)$$

[3]Bold symbols denote matrixes.

Accordingly, the log-likelihood function is

$$l(\theta) = -\frac{1}{2\sigma_S^2}\sum_{k=1}^{K}\sum_{n=1}^{N_k}\left(\overline{PL}_{kn} - g_{kn}(\theta)\right)^2, \quad (14)$$

and the Fisher matrix can be expressed as

$$[\mathbf{F}]_{ij} = -E\left[\frac{\partial^2 l(\theta)}{\partial\theta_i \partial\theta_j}\right] = \frac{1}{\sigma_S^2}\sum_{k=1}^{K}\sum_{n=1}^{N_k}\frac{\partial g_{kn}(\theta)}{\partial\theta_i}\frac{\partial g_{kn}(\theta)}{\partial\theta_j}. \quad (15)$$

The $\mathbf{F}$ can consequently be evaluated from the partial derivatives of the estimator, which are

$$\frac{\partial g_{kn}(\theta)}{\partial x} = \frac{10\,(x_T - x_{kn})}{\ln(10)} \cdot \frac{\gamma_k}{d_{kn}^2}, \quad (16)$$

$$\frac{\partial g_{kn}(\theta)}{\partial y} = \frac{10\,(y_T - y_{kn})}{\ln(10)} \cdot \frac{\gamma_k}{d_{kn}^2}, \quad (17)$$

$$\frac{\partial g_{kn}(\theta)}{\partial \gamma_k} = \frac{10}{\ln(10)} \cdot \ln(d_{kn}), \quad (18)$$

$$\frac{\partial g_{kn}(\theta)}{\partial L_k} = 1. \quad (19)$$

Lastly, the CRLBs on the estimation errors are evaluated as

$$e_{rms}^2 \geq \left[\mathbf{F}^{-1}\right]_{11} + \left[\mathbf{F}^{-1}\right]_{22}, \quad (20)$$

$$\sigma_{\gamma_k}^2 \geq \left[\mathbf{F}^{-1}\right]_{2+k,2+k}, \quad (21)$$

$$\sigma_{L_k}^2 \geq \left[\mathbf{F}^{-1}\right]_{2+K+k,2+K+k}, \quad (22)$$

where e_{rms}^2, $\sigma_{\gamma_k}^2$, $\sigma_{L_k}^2$ are the bounds on the location errors, γ_k and L_k respectively. Accordingly, the root mean square error (RMSE) on the location is $e_{rms} = \sqrt{(x_T - \hat{x}_T)^2 + (y_T - \hat{y}_T)^2}$, whereas the errors on the PL parameters are $\sigma_{\gamma_k} = |\gamma_k - \hat{\gamma}_k|$ and $\sigma_{L_k} = \left|L_k - \hat{L}_k\right|$. In Fig. 5, the average RMSEs returned by the proposed algorithm are compared with the CRLB for two values of σ_S. We randomly generate the anchor points' positions once and keep them fixed to assess the effects of the σ_S on the errors. On average, the algorithm achieves the CRLB independently from the shadowing, though the noise increases the minimum theoretical achievable errors.

B. Multi-slope PL

We examine the accuracy of the considered algorithm in the case of a dual-slope PL. The anchor's positions are randomly generated at each iteration, and $d_2^{(c)} = 50$ m is set. We give the algorithm firstly the correct value of $d_2^{(c)}$ and, secondly, a wrong value $d_2^{(c)} = 75$ m as input.

If the algorithm knows the exact $d_2^{(c)}$, it achieves the CRLB (Fig. 6). Obliviously, a wrong value of $d_2^{(c)}$ increases the algorithm's errors. In particular, the location error increases significantly if a single-slope is assumed when running the algorithm, remarking the importance of a valid assumption on the radio propagation of the area. Instead, the algorithm is quite robust to errors on the critical distances if the number of measurements is high enough. For instance, the location RMSE is still lower than 1 m for $M \geq 140$.

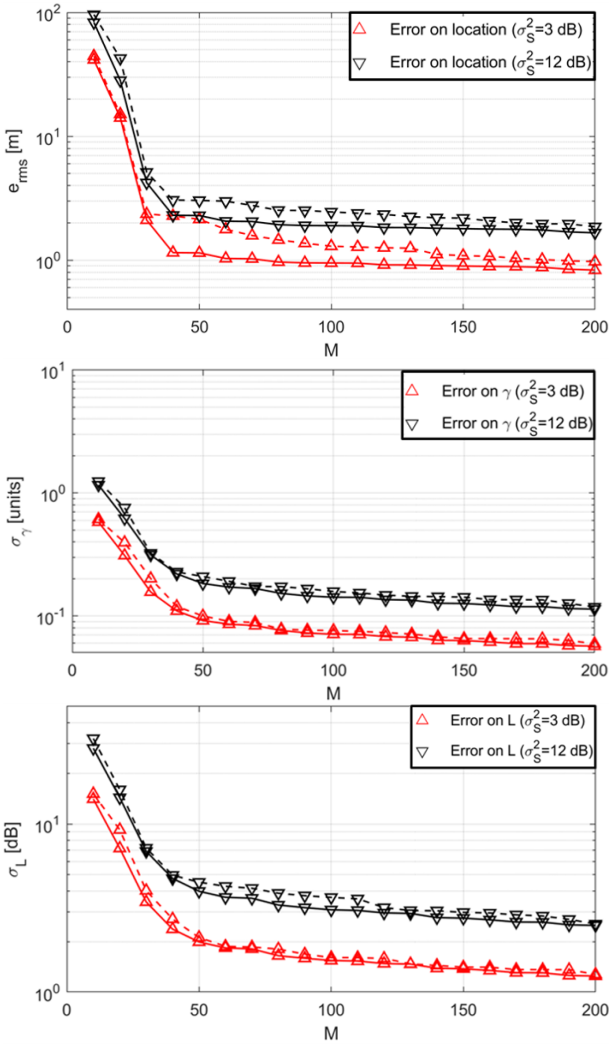

Fig. 5. Performance of the proposed localization algorithm (dashed lines) compared with the CRLB (continuous lines) for $\sigma_S^2 = 3$ dB and $\sigma_S^2 = 12$ dB.

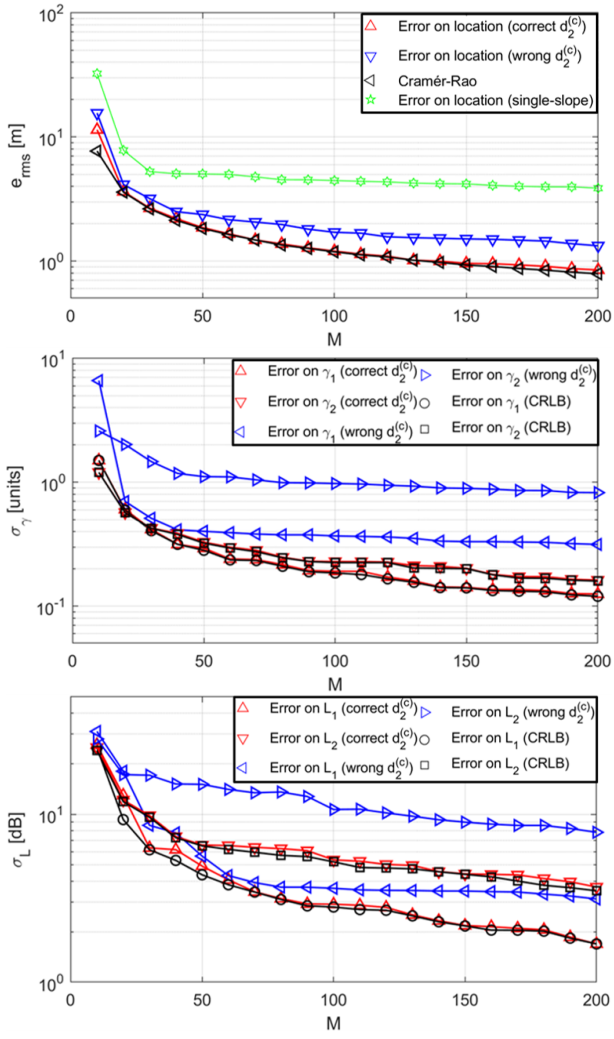

Fig. 6. Performance of the proposed localization algorithm compared with the CRLB in the dual-slope case when the input $d_2^{(c)}$ value is either correct ($d_2^{(c)} = 50$ m) or wrong ($d_2^{(c)} = 75$ m).

C. Angular Dependent PL

Finally, we apply the algorithm in the case of an angular dependent PL. We divide the search area into two equal angular sectors, each characterized by a different PLE. The e_{rms} for $M = 100$ and $M = 200$ are compared to the CRLB in Fig. 7 when the error on the assumed $\delta_2^{(c)}$ increases up to 15°. Even in this case, the error is similar to the CRLB if the $\delta_2^{(c)}$ is known. Interestingly, an error as low as 2.5° appears to nullify the benefit of a higher number of collected RSS measurements when $M \geq 100$, and a sectorization error higher than 5° results in the failure of the algorithm. Due to the wrong data partitioning, the RSS-based localization in scenarios characterized by an angular dependent PL is thus more critical than in the case of a multi-slope PL since a slightly incorrect $\delta_2^{(c)}$ causes high errors on the target's location. The partitioning precision is expected to be particularly relevant when employing sectorized antennas [2] for the RSS-based localization.

VII. Experimental Results

The proposed algorithm is tested in a real scenario wherein a dual-slope PL model is expected. The transmitting and the receiving radios consist of Arduino Uno boards and Dragino LoRa shields connected to 868 MHz dipoles. The transmitting board is programmed to transmit one LoRa packet every 3 seconds (LoRa transmission parameters as in [51]). Horizontally polarized electromagnetic waves are exploited, and the transmitting radio is placed on the ground. A 62 m × 58 m area, including a building of the University of Rome Tor Vergata, is selected as the test area, as detailed in Fig. 8. A network composed of five moving anchor points is then set up. Each receiving board is carried by a volunteer along a straight-line path and sends measured RSSI and SNR to a laptop via Wi-Fi, then the PL is evaluated according to (3). Every PL measurement is averaged on three packets so that 200 measurements are collected in 6 minutes. Due to the anchor points positions, a dual-slope PL is experienced, one for the outdoor (receivers 1,

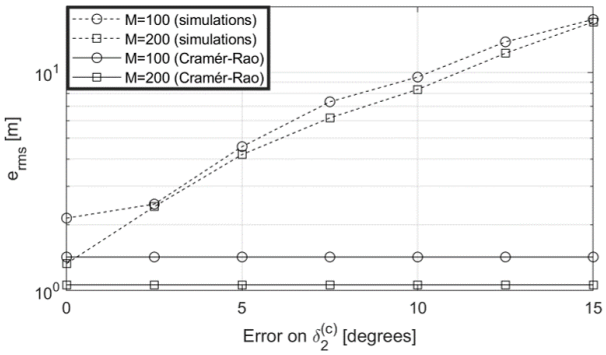

Fig. 7. Performance of the proposed localization algorithm compared with the CRLB in the case of two angular sectors having different PL when increasing the error on the input $\delta_2^{(c)}$ value.

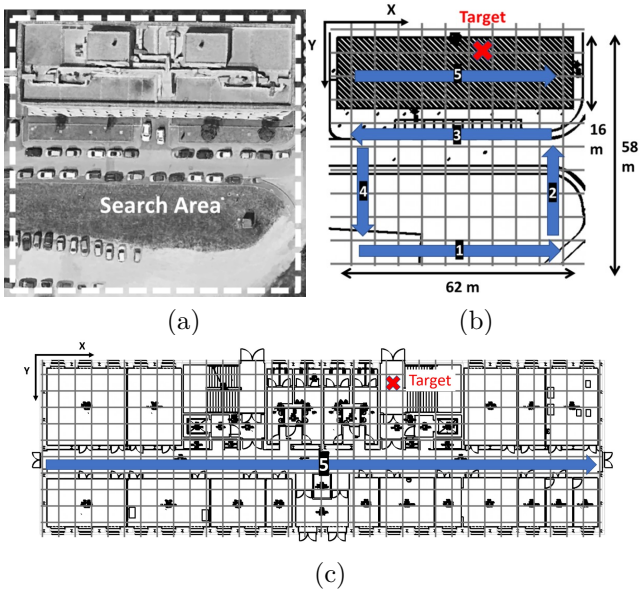

Fig. 8. Search area and transmitter location selected for the experimentation of the localization algorithms. (a) Satellite image of the search area, (b) sketch of a grid superimposed over the search area, and (c) planimetry of the indoor environment considered. The target position and the paths of the five numbered receivers are shown.

2, 3, and 4) and one for the indoor (receiver number 5) environments.

Based on the search area analysis and the anchor points' topology, since the indoor area is 16 m × 62 m, the algorithm is set to search for the critical distance between 5 m and 40 m using a step of 5 m. The data are given as input to four localization algorithms simultaneously: the proposed algorithm, an RSS-UDPG ESA estimating (x_T, y_T) and L fixed γ exhaustively searched [25], the GN RSS-UDPG algorithm [34], and a classic RSS-based ESA assuming free-space PL [38]. After 6 minutes, the error on the location returned by the presented algorithm is 5 m, significantly outperforming the methods which assume a single slope and return errors comprised between 12 m and 47 m (Fig. 9). It is worth noticing that the experimental data are affected by a very high noise due to misalignments between the transmitting and receiving dipoles, resulting

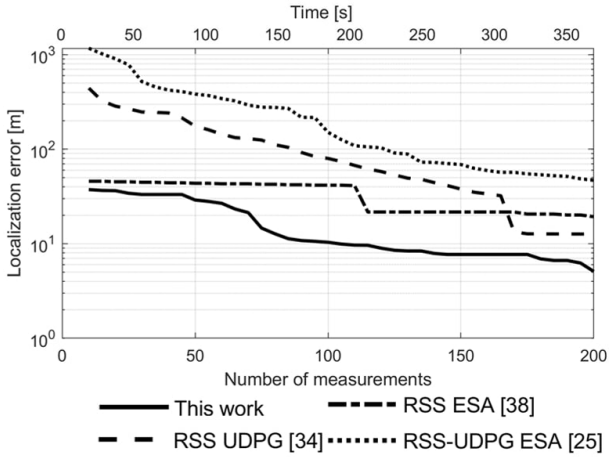

Fig. 9. Experimental localization errors returned by the four tested algorithms.

in variable polarization losses and values of the gains. Because of this additional noise, the RSS measurement can be considered affected by an extremely high shadow fading. In practical applications, the additional noise can be reduced with near-isotropic antennas and employing linear and circularly polarized electromagnetic waves to make the polarization losses constant and equal to −3 dB. When considering the STDs numerically evaluated and the uncertainty on the unknown $d_2^{(c)}$, the error is coherent with the simulations shown in Fig. 5 and Fig. 6.

Six minutes could be an excessive long localization time for some applications. It should be noticed that this long time is due to the duty cycle imposed by the LoRa protocol [17], [52], which influenced the maximum packet rate achievable by the transceiver used in the experiment. We report the run times of the considered optimization techniques in Fig. 10 corresponding to calculations based on experimental data and those obtained by simulation. Data in Fig. 10 are obtained considering the hardware/software settings in Table V and the test area in Fig. 8. Naturally, the ESAs' run times are mostly unaffected by the datasets, unlike the GN-based nonlinear technique. The proposed algorithm performed similarly to traditional methods and registered a maximum run time of 600 ms during the experiment. In the case of no exhaustive search over the critical distance, the run time is only slightly higher than the one of the RSS ESA. Therefore, in realistic operative conditions, the localization time is expected to be determined by the measurement period. The measurements can be speeded up by employing a high number of anchor points. If the measurement time is in the same order of magnitude as the lowest run time of the proposed method in Fig. 10, localization with 200 experimental data is carried out in about 20 seconds.

VIII. Conclusion and Future Directions

This paper introduced and analyzed an ESA for RSS-UDPG localization of a transmitter in a search area covered by a radio network. Thanks to an exhaustive

TABLE V
HARDWARE AND SOFTWARE UTILIZED FOR THE RUN TIMES EVALUATION.

Central processing unit	Intel® Core i7-9700KF	**Processor frequency**	3.60 GHz
Random-access memory	16 GB	**Software**	Matlab® R2019b

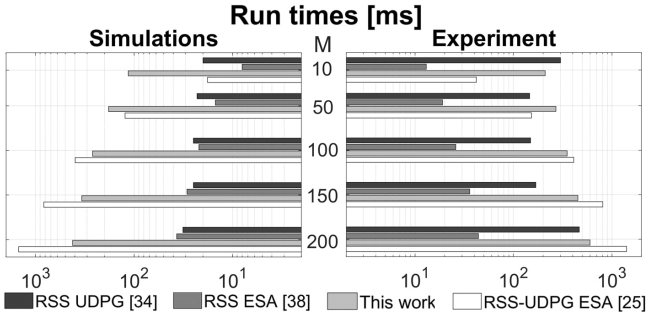

Fig. 10. Run time of the four tested algorithms when employing simulated or experimental PL values.

search of the transmitter's candidate positions, the PL parameters are evaluated analytically. The position estimation algorithm can achieve the CRLB in every propagation scenario, including complex multi-slope and angular dependent PL models. Interestingly, angular dependent PL scenarios resulted in being the most critical case. According to simulations, the method allows achieving good accuracy even for a relatively small number of RSS measurements. The algorithm was tested in a network composed of 5 moving anchor points covering both outdoor and indoor areas. From the test exploiting very noisy RSS measurement, the algorithm returns a localization error of 5 m with 200 PL measurements, while classic techniques assuming a single slope are affected by errors up to 47 m.

Before concluding the paper, it could be of interest to outline some future directions of this research. Data partitioning could be optimized to improve the accuracy of the position estimate. To this purpose, the optimization of the piecewise-linear approximation [53] or unsupervised data clustering [54] could be exploited. However, the overall run time of the algorithm should be kept short. Another interesting topic is the simultaneous localization of multiple transmitters in a complicated radio propagation environment, wherein it is not possible to cluster similar measured PL based only on the RSS [55]. In this case, hybrid methods also exploiting DoA [2] or ToA [56] could be helpful to overcome this challenge by combining information from the different signal sources to benefit the network localization.

REFERENCES

[1] G. Mao, *Localization Algorithms and Strategies for Wireless Sensor Networks*. Hershey, NY, USA: Information Science Reference, 2009.

[2] J. Werner, J. Wang, A. Hakkarainen, D. Cabric, and M. Valkama, "Performance and Cramer-Rao bounds for DoA/RSS estimation and transmitter localization using sectorized antennas," *IEEE Trans. Veh. Technol.*, vol. 65, no. 3, pp. 3255–3270, May 2016.

[3] H. Naseri and V. Koivunen, "A bayesian algorithm for distributed network localization using distance and direction data," *IEEE Trans. Signal Inf. Process. Netw.*, vol. 5, no. 2, pp. 290–304, June 2019.

[4] C. Cavarese, J. M. Rabaey, and J. Beutel, "Location in distributed ad-hoc wireless sensor networks," in *2001 IEEE Int. Conf. Acoust., Speech, Signal Process.*, Salt Lake City, UT, USA, 2001, pp. 2037–2040.

[5] J. H. Lee and R. M. Buehrer, "Fundamentals of received signal strength-based position location," in *Handbook of Position Location: Theory, Practice, and Advances*, 1st ed. Hoboken, NJ, USA: John Wiley and Sons, 2012, ch. 11, pp. 359–395.

[6] R. J. R. Thompson, E. Cetin, and A. G. Dempster, "Unknown source localization using RSS in open areas in the presence of ground reflections," in *Proc. 2012 IEEE/ION Position, Location Navigation Symp.*, Myrtle Beach, SC, USA, Apr. 2012, pp. 1018–1027.

[7] A. Vazquez-Rodas, F. Astudillo-Salinas, C. Sanchez, B. Arpi, and L. I. Minchala, "Experimental evaluation of RSSI-based positioning system with low-cost LoRa devices," *Ad Hoc Netw.*, vol. 105, Aug. 2020, Art. no. 102168.

[8] X. Ge, S. Tu, G. Mao, C. Wang, and T. Han, "5G Cellular Networks," *IEEE Wireless Commun.*, vol. 23, no. 1, pp. 72–79, Feb. 2020.

[9] A. S. Martinez-Sala, F. Losilla, J. C. Sánchez-Aarnoutse, and J. García-Haro, "Design, implementation and evaluation of an indoor navigation system for visually impaired people," *Sensors*, vol. 15, no. 12, pp. 32 168–32 187, Dec. 2015.

[10] A. Boukerche, H. A. Oliveira, E. F. Nakamura, and A. A. Loureiro, "Vehicular ad hoc networks: a new challenge for localization-based systems," *Comput. Commun.*, vol. 31, no. 12, pp. 2838–2849, July 2018.

[11] N. Saeed, W. Ahmad, and D. M. S. Bhatti, "Localization of vehicular ad-hoc networks with RSS based distance estimation," in *2018 Int. Conf. Comput., Math. Eng. Technol.*, Sukkur, Pakistan, Mar. 2018, pp. 1–6.

[12] K. Derr and M. Manic, "Wireless based object tracking based on neural networks," in *3rd IEEE Conf. on Industrial Electronics Appl.*, Singapore, Singapore, Jun. 2008, pp. 308–313.

[13] D. Ciuonzo, P. S. Rossi, and P. K. Varshney, "Distributed detection in wireless sensor networks under multiplicative fading via generalized score tests," *IEEE Internet of Things Journal*, vol. 8, no. 11, pp. 9059–9071, Nov. 2021.

[14] D. Ciuonzo and P. S. Rossi, "Distributed detection of a non-cooperative target via generalized locally-optimum approaches," *Information Fusion*, vol. 36, pp. 261–274, Jul. 2017.

[15] A. Shoari and A. Seyedi, "Detection of a non-cooperative transmitter in Rayleigh fading with binary observations," in *2012 IEEE Military Communications Conference*, Orlando, FL, USA, Nov. 2012, pp. 1–5.

[16] J. Wang, H. Liu, H. Bao, B. Bennett, and C. Flores-Montoya, "Target localization and navigation with directed radio sensing in wireless sensor networks," in *Proc. Internet of Veh. - Safe Intell. Mobility Conf.*, Chengdu, China, Dec. 2015, pp. 101–113.

[17] G. M. Bianco, R. Giuliano, G. Marrocco, F. Mazzenga, and A. Mejia-Aguilar, "LoRa system for search and rescue: path loss models and procedures in mountain scenarios," *IEEE Internet Things J.*, vol. 8, no. 3, pp. 1985–1999, Feb. 2021.

[18] S. Shrestha, J. Talvitie, and E. S. Lohan, "Deconvolution-based indoor localization with WLAN signals and unknown access point locations," in *2013 Int. Conf. Localization GNSS*, Turin, Italy, June 2013, pp. 1–6.

[19] M. Raspopoulos *et al.*, "Location-dependent information extraction for positioning," in *2012 Int. Conf. Localization GNSS*, Starnberg, Germany, June 2012, pp. 1–6.

[20] A. Hrovat, G. Kandus, and T. Javornik, "A survey of radio propagation modeling for tunnels," *IEEE Commun. Surv. Tutor.*, vol. 16, no. 2, pp. 658–669, Oct. 2014.

[21] A. E. Forooshani, S. Bashir, D. G. Michelson, and S. Noghanian, "A survey of wireless communications and propagation modeling in underground mines," *IEEE Commun. Surv. Tut.*, vol. 15, no. 4, pp. 1524–1545, Mar. 2013.

[22] M. U. Sheikh, K. Hiltunen, and J. Lempiäinen, "Angular wall loss model and extended building penetration model for outdoor to indoor propagation," in *13th Int. Wireless Commun. Mobile Comput. Conf.*, Valencia, Spain, June 2017, pp. 1291–1296.

[23] C. Larsson, B. Olsson, and J. Medbo, "Angular resolved pathloss measurements in urban macrocell scenarios at 28 GHz," in *IEEE 84th Veh. Technol. Conf.*, Montréal, Canada, June 2016, pp. 1–5.

[24] N. Salman, A. H. Kemp, and M. Ghogho, "Low complexity joint estimation of location and path-loss exponent," *IEEE Wireless Commun. Lett.*, vol. 1, no. 4, pp. 364–367, Aug. 2012.

[25] Y. T. Chan, B. H. Lee, R. Inkol, and F. Chan, "Estimation of emitter power, location, and path loss exponent," in *Proc. 25th IEEE Can. Conf. Elect. Comput. Eng.*, Montreal, Canada, Apr. 2012, pp. 1–5.

[26] ——, "Received signal strength localization with an unknown path loss exponent," in *Proc. 24th Can. Conf. Elect. Comput. Eng.*, Niagara Falls, Canada, May 2011, pp. 456–459.

[27] J. Shirahama and T. Ohtsuki, "RSS-based localization in environments with different path loss exponent for each link," in *Proc. IEEE Veh. Technol. Conf.*, Singapore, Singapore, May 2008, pp. 1509–1513.

[28] I. Yamada, T. Ohtsuki, T. Hisinaga, and L. Zheng, "An indoor location estimation method by maximum likelihood algorithm using RSS," in *SICE Annual Conference*, Tamakatsu, Japan, Sep. 2007, pp. 2927–2930.

[29] M. R. Gholami, R. M. Vaghefi, and E. G. Strom, "RSS-based sensor localization in the presence of unknown channel parameters," *IEEE Trans. Signal Process.*, vol. 61, no. 15, pp. 3752–3759, Aug. 2013.

[30] G. Wang, H. Chen, Y. Li, and M. Jin, "On received-signal-strength based localization with unknown transmit power and path loss exponent," *IEEE Wireless Commun. Lett.*, vol. 1, no. 2, pp. 536–539, Oct. 2012.

[31] H. Nurminem *et al.*, "Statistical path loss parameter estimation and positioning using RSS measurements in indoor wireless networks," in *Proc. 2012 Int. Conf. Indoor Positioning Indoor Navigation*, Sydney, Australia, Nov. 2012, pp. 1–9.

[32] A. Bel, J. L. Vicario, and G. Seco-Granados, "Localization algorithm with on-line path loss estimation and node selection," *Sensors*, vol. 11, no. 7, pp. 6905–6925, Jul. 2011.

[33] S. Chang, Y. Li, H. Wang, and G. Wang, "Received signal strength-based target localization under spatially correlated shadowing via convex optimization relaxation," *Int. J. Distrib. Sensor Netw.*, vol. 14, no. 6, June 2018.

[34] X. Li, "RSS-based location estimation with unknown pathloss model," *IEEE Trans. Wireless Commun.*, vol. 5, no. 12, pp. 3626–3633, Dec. 2006.

[35] N. Salman, M. Ghogho, and A. H. Kemp, "On the joint estimation of the RSS-based location and path-loss exponent," *IEEE Wireless Commun. Lett.*, vol. 1, no. 1, pp. 34–37, Feb. 2012.

[36] S. Uluskan and T. Filik, "A geometrical closed form solution for RSS based far-field localization: direction of exponent uncertainty," *Wireless Netw.*, vol. 25, no. 3, pp. 215–227, July 2019.

[37] R. Sari and H. Zayyani, "RSS localization using unknown statistical path loss exponent model," *IEEE Commun. Lett.*, vol. 22, no. 9, pp. 1830–1833, Sep. 2018.

[38] A. J. Weiss, "On the accuracy of a cellular location system based on RSS measurements," *IEEE Trans. Veh. Technol.*, vol. 52, no. 6, pp. 1508–1518, Nov. 2003.

[39] A. Dogandzic and P. P. Amran, "Signal-strength based localization in wireless fading channels," in *Proc. Conf. Rec. 38th Asilomar Conf. Signals, Syst. Comput.*, Pacific Grove, CA, USA, Nov. 2004, pp. 2160–2164.

[40] K. Pahlavan and A. Levesque, *Wireless Information Networks*, 2nd ed. New York, NY, USA: Wiley, 2005.

[41] G. Soatti, M. Nicoli, S. Savazzi, and U. Spagnolini, "Consensus-based algorithms for distributed network-state estimation and localization," *IEEE Trans. Signal Inf. Process. Netw.*, vol. 3, no. 2, pp. 430–444, June 2017.

[42] G. Mao, B. D. Anderson, and B. Fidan, "Path loss exponent estimation for wireless sensor network localization," *Comput. Netw.*, vol. 51, no. 10, pp. 2467–2483, July 2007.

[43] Y. Zou and H. Liu, "RSS-based target localization with unknown model parameters and sensor position errors," *IEEE Trans. Veh. Technol.*, vol. 70, no. 7, pp. 6969–6982, Jun. 2021.

[44] A. Goldsmith, *Wireless Communication*, 1st ed. Cambridge, U.K.: Cambridge University Press, 2005.

[45] D. Åkerberg, "Properties of a TDMA pico cellular office communication system," in *IEEE Veh. Technol. Conf.*, San Francisco, CA, USA, May 1989, pp. 186–191.

[46] M. Babalou, S. Alirezaee, A. Soheili, A. Ahmadi, M. Ahmadi, and S. Erfani, "Microcell path loss estimation using log-normal model in GSM cellular network," in *Int. Symp. Signals, Circuits Systems*, Iasi, Romania, Aug. 2015, pp. 1–4.

[47] J.-J. Park, J. Lee, K.-W. Kim, and M.-D. Kim, "Large- and small-scale fading characteristics of mmWave HST propagation channel based on 28-GHz measurements," in *15th European Conf. Antennas Propag.*, Dusseldorf, Germany, Mar. 2021, pp. 1–5.

[48] P. Zhang, H. Wang, and W. Hong, "Empirical analysis of millimeter-wave propagation in indoor transitional environments," in *IEEE Int. Symp. Antennas Propag. North American Radio Sci. Meeting*, Montreal, Canada, Jul. 2020, pp. 1189–1190.

[49] K. Nuangwongsa, K. Phaebua, T. Lertwiriyaprapa, C. Phongcharoenpanich, and M. Krairiksh, "Path loss modeling in durian orchard for wireless network at 5.8 GHz," in *6th Int. Conf. Electrical Eng./Electronics, Computer, Telecom. Inf. Technol.*, Chonburi, Thailand, May 2009, pp. 816–819.

[50] Y. Zhang, G. Zheng, and J. Sheng, "Radio propagation at 900 MHz in underground coal mines," *IEEE Transactions on Antennas and Propagation*, vol. 49, no. 5, pp. 757–762, May 2001.

[51] G. M. Bianco, A. Mejia-Aguilar, and G. Marrocco, "Performance evaluation of LoRa LPWAN technology for mountain search and rescue," in *5th Int. Conf. Smart Sustain. Technol.*, Split, Croatia, 2020, pp. 1–4.

[52] D. Zorbas, "Design considerations for time-slotted LoRa(WAN)," in *Proc. 2020 Int. Conf. Embedded Wireless Systems Netw.*, Lyon, France, Feb. 2020, pp. 271–276.

[53] S. Rebennack and J. Kallrath, "Continuous piecewise linear delta-approximations for univariate functions: Computing minimal breakpoint systems," *J. Optim. Theory Appl.*, vol. 167, no. 2, pp. 617–643, 2015.

[54] S. Bandyopadhyay and S. Saha, *Unsupervised classification: Similarity measures, classical and metaheuristic approaches, and applications*, 1st ed. Berlin, Germany: Springer, 2013.

[55] M. Saadati and J. Nelson, "Multiple transmitter localization using clustering by likelihood of transmitter proximity," in *Conf. Record 51st Asilomar Conf. on Signals, Systems and Computers*, Oct. 2018, pp. 1769–1773.

[56] A. Coluccia and A. Fascista, "Hybrid TOA/RSS range-based localization with self-calibration in asynchronous wireless networks," *Journal of Sensor and Actuator Networks*, vol. 8, no. 2, May 2019.